ELSEVIER

Journal of Nuclear Materials 312 (2003) 67–75

journal of nuclear materials

www.elsevier.com/locate/jnucmat

Electron backscatter diffraction of a plutonium–gallium alloy

C.J. Boehlert [a,*], T.G. Zocco [b], R.K. Schulze [b], J.N. Mitchell [b], R.A. Pereyra [b]

[a] *School of Ceramic Engineering and Materials Science, Alfred University, 2 Pine Street, Alfred, NY 14802, USA*
[b] *Nuclear Materials Technology Division, Los Alamos National Laboratory, Los Alamos, NM 87545, USA*

Received 27 August 2002; accepted 15 October 2002

Abstract

An experimental technique has recently been developed to characterize reactive metals, including plutonium (Pu) and cerium, using electron backscatter diffraction (EBSD). Microstructural characterization of Pu and its alloys by EBSD had been previously elusive primarily because of the extreme toxicity and rapid surface oxidation rate associated with Pu metal. The experimental technique, which included ion-sputtering the metal surface using a scanning Auger microprobe (SAM) followed by vacuum transfer of the sample from the SAM to the scanning electron microscope (SEM), used to obtain electron backscatter diffraction Kikuchi patterns and orientation maps for a Pu–gallium alloy is described and the initial microstructural observations based on the analysis are discussed. The phase transformation behavior between the δ (face-centered cubic) and ε (body-centered-cubic) structures is explained by combining the SEM and EBSD observations.

PACS: 07.78.+s; 61.16.Bg

1. Introduction

Plutonium (Pu) is one of the most reactive metals, and its outer surface reacts vigorously with oxygen, hydrogen, and water [1–3]. Due to Pu's radioactive nature, self-irradiation damage is constantly affecting its internal microstructure. This extreme reactivity of Pu makes metallurgical characterization challenging. Various microscopy characterization techniques, including optical microscopy, scanning electron microscopy (SEM), and transmission electron microscopy (TEM) have been useful for understanding the nature of its reactivity as well its microstructural evolution and phase transformation behavior [4–9]. A more recently developed electron microscopy-based characterization technique, automated electron backscatter diffraction (EBSD) orientation mapping, has proven to be a powerful method for characterizing orientation relationships, texture, phase transformations, grain boundary misorientations, phase identification, etc. for a variety of metals and alloys [10,11]. EBSD orientation mapping is a SEM-based technique for the collection and indexing of electron backscatter Kikuchi patterns (EBSPs), and it allows for the collection of a large number of grain orientation measurements in a relatively short period of time. Due to the complex phase transformation behavior of Pu, which experiences six allotropic phases from room temperature (RT) to 640 °C (see Fig. 1), EBSD would be useful for addressing some of the many questions concerning microstructural evolution and phase transformation behavior of Pu and its alloys.

An experimental technique has been developed to capture EBSPs for reactive metals including Pu and cerium (Ce) [13,14]. This specialized technique is necessary to avoid formation of an amorphous surface oxide layer, which rapidly forms when reactive metals are exposed to the atmosphere. This thick oxide layer prevents the release and capture of elastically backscatter electrons, which provide structural information, from the underlying crystalline metal. In this work, the initial EBSD orientation maps of a Pu alloy were obtained and both

* Corresponding author. Tel.: +1-607 871 2906; fax: +1-607 871 3047.
E-mail address: boehlecj@alfred.edu (C.J. Boehlert).

0022-3115/03/$ - see front matter
PII: S0022-3115(02)01555-6

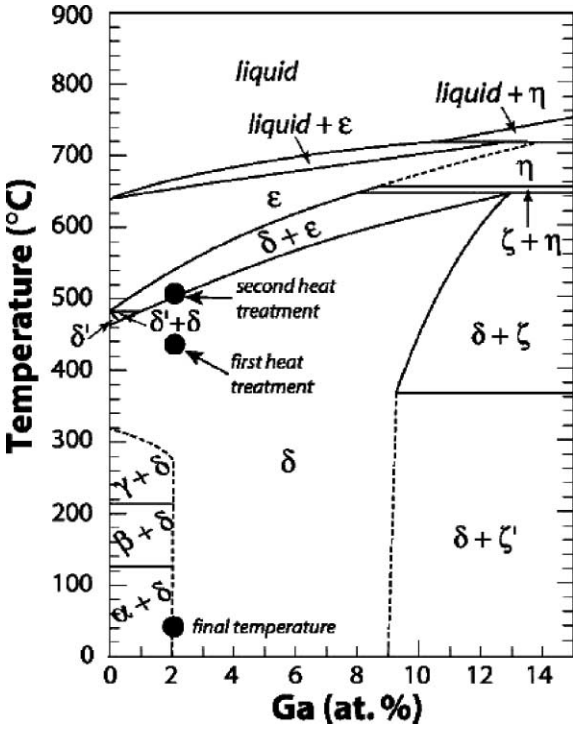

Fig. 1. The Pu–Ga phase diagram (adapted from Peterson and Kassner [12]) highlighting the sample's thermal history.

the experimental technique and preliminary microstructural analysis are discussed. Pu was alloyed with gallium (Ga) to stabilize the face-centered cubic (fcc) δ-phase structure (Fig. 1). The alloy underwent a heat treatment within the $\varepsilon + \delta$ phase field and the microscopy observations provided evidence of the phase transformation behavior.

2. Experimental technique

The Pu–Ga alloy used in this study had a nominal Ga composition of 2 at.% and was heat treated at 440 °C for 12 h to obtain a fully-stabilized δ-phase microstructure. The alloy was then heated within the two-phase $\varepsilon + \delta$ region followed by quenching into the δ-phase field followed by slow cooling to RT. The heat treatment is represented in Fig. 1. Samples were cut using a slow-speed diamond saw and PF-5070 (3M Brand Performance Fluid) as a lubricant. The samples were mounted, ground, and polished to a final thickness of less than 500 μm. The final polishing step included 1 μm diamond paste on a nappy cloth using De-Solve-It (orange peel oil in a mineral oil base solution) as a lubricant. All the above metallurgical operations were performed in a glovebox to prevent spread of Pu dust and contamination. TEM disks were punched and electropolished in a solution of 10% nitric acid and 90% dimethylformamide at −13 °C, 18 V, and 80 mA using a twin-jet Struers Tenupol-3 polishing unit. To avoid the large dished surface characteristic of a TEM sample, electropolishing was performed for only 1 min and the sample was not perforated. The electropolished sample was then mounted on a specially-designed puck containing a 3 mm-diameter recess to accept the disk (for illustration see reference [13]). The sample was then placed in the SEM and EBSPs of the polycrystalline underlying metal were not observed, which was believed to be a result of the surface oxide layer which grew during the exposure to atmosphere. This necessitated a means to remove the oxide layer from the surface.

A freshly prepared sample was then placed on the puck and the sample-puck-platform assembly was inserted into a Physical Electronics 4100 scanning Auger microprobe (SAM) which was used to both characterize the surface chemistry through Auger spectroscopy as well as remove the surface contaminant layers via ion-sputtering in vacuum (9×10^{-9} Torr). Fig. 2 shows the Auger spectra, using 5 keV incident electrons, taken from the surface of the sample. Note that in addition to Pu peaks, carbon (C) and oxygen (O) peaks were observed. The sampling depth of the Auger electrons was estimated to be 4.5 nm and based on the intensity of the O peak, the oxide layer was at least as thick as the sampling depth. To remove these surface contaminants, the sample was tilted such that the ion gun was oriented

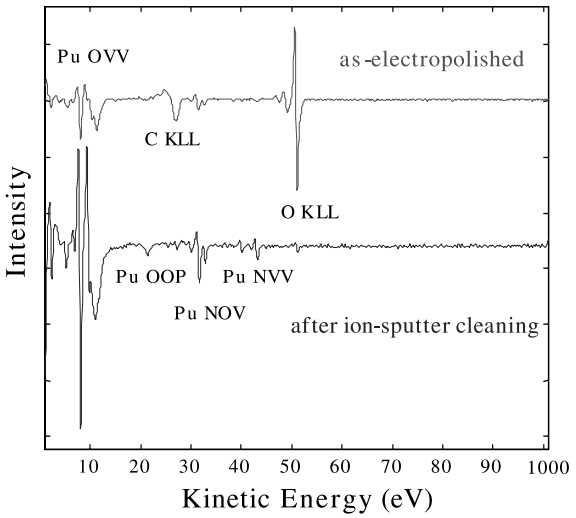

Fig. 2. Differential Auger spectra before and after Ar ion-sputtering of the sample surface. The peak-to-peak intensity is indicative of relative elemental concentrations and the OVV, KLL, OOP, NVV, and NOV labels refer to the origin of the spectral Auger transition. Note the significant reduction in the carbon (C) and oxygen (O) peaks and the increased height of the Pu peaks after sputter cleaning.

approximately 25° from the sample normal and 4 keV argon (Ar) ions at a current density of 55 μA/cm^2 bombarded the sample surface for 10 min. As a result, the C and O peaks were significantly reduced. Note that all of the ion-sputtering was unidirectional relative to the surface. Ar ion bombardment at 4 keV would induce a steady-state surface damage layer approximately 5 nm thick as estimated by TRIM (TRansport of Ions in Matter) software using Monte Carlo-based simulations [15]. A second sputtering step (10 min with 500 eV Ar ions at 9 μA/cm^2) was performed to reduce the depth of the damage layer caused by the initial sputtering run. The estimated final surface damage layer caused by the 500 eV ions was approximately 1 nm thick. Fig. 2 compares the resulting Auger spectra with that for the as-electropolished material before sputtering. Note the significant reduction in the O and C peaks and the increased height of the Pu peaks for the sputtered condition compared to the as-electropolished condition. Based on peak height analysis, the atomic concentration of O at the surface was reduced by a factor greater than three. In this respect the multifunctional SAM proved to be more valuable than a simple ion-etcher as it not only provided sputtering capability in a high-vacuum atmosphere, but it also was able to identify and semi-quantitatively analyze the surface contaminants.

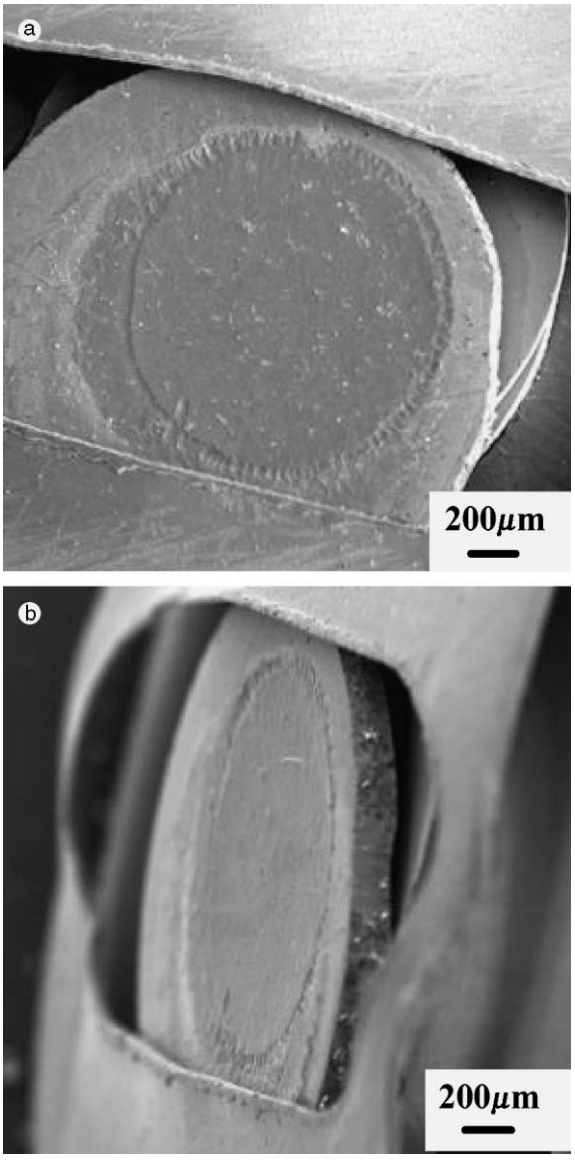

Fig. 3. Images of the electropolished and ion-sputtered sample in the SEM chamber. The sample could be tilted (a) nearly normal to the electron beam and (b) at 70° with respect to the electron beam, which is optimal for EBSD.

Using a vacuum suitcase to minimize surface oxidation, the sample was then transferred from the SAM to a JEOL JSM-6300FXV field-emission (FE) SEM using the procedures described in Boehlert et al. [13]. It is noted that the vacuum transfer is a requirement as the authors have observed that exposure of the sample to atmosphere for even 1 s prevented successful EBSD capture [13]. The transfer time was approximately 15 min, and the highest pressure the sample experienced was 4×10^{-6} Torr. Once inside the SEM chamber, see Fig. 3(a) and (b), the sample was maintained at a constant atmosphere of 4×10^{-7} Torr. The SEM stage tilt allowed a range of 0–85° for the angle formed between the sample normal and the electron beam. An angle of 70° was optimal for EBSP capture. The EBSPs were obtained using an accelerating voltage of 30 keV and 1–3 nA of specimen absorbed current. The orientation maps were performed using a step size of 1 μm. EDAX-TSL, Inc., Draper, Utah manufactured the EBSD hardware and software. The δ-phase fcc structure in the Pu–Ga alloy has a lattice parameter of approximately 0.463 nm as measured by XRD.

3. Results

After the initial heat treatment (440 °C) within the δ-phase field, the Pu–Ga alloy exhibited an equiaxed fully-δ phase microstructure with the grain size ranging between 20 and 40 μm. During the subsequent heat treatment, which included a brief excursion into the $\delta + \varepsilon$ phase regime, a small portion of the original δ-phase grains (or parent δ grains) transformed to ε (bcc structure). The transformation occurred primarily at the parent δ-phase grain boundaries. Upon cooling to the δ-phase field, the ε grains transformed back to the δ phase leaving a fine distribution of δ grains at the parent δ grain boundaries. Fig. 4 depicts an optical photomicrograph of the post heat-treatment microstructure. In addition to a distribution of inclusions, there was a

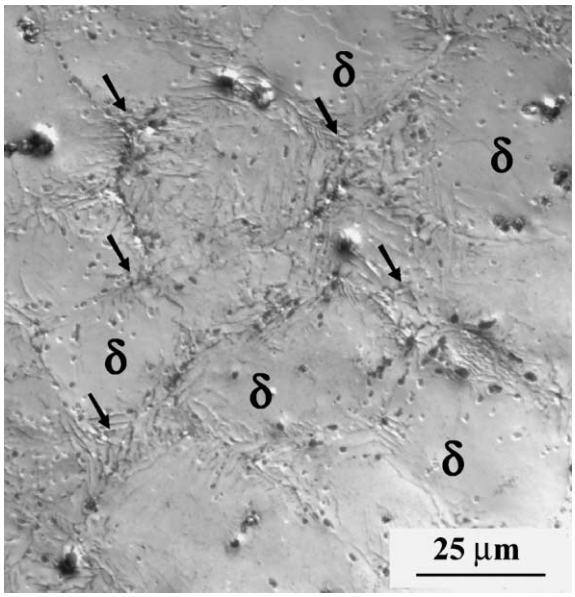

Fig. 4. Optical photomicrograph of the Pu–Ga alloy microstructure with arrows indicating the transformed regions at the parent δ grain boundaries.

bimodal distribution of δ-phase grain sizes. The widths of the transformed grains, which tended to be slightly elongated so their appearance was more lenticular than equiaxed, were on the order of a few microns or less. Fig. 5(a) and (b) are representative SEM images of the microstructure following ion-sputtering.

When choosing the areas for EBSD orientation mapping, the regions of the sample containing visible protrusions were avoided (see Fig. 6). The surface protrusions formed as a result of the different surface removal rates associated with electropolishing and ion sputtering the inclusions within the Pu–Ga metal. The number and height of the protrusions can be reduced by minimizing the sputtering time, which is directly related to the cleanliness of the surface as discussed in the discussion section.

Fig. 7 illustrates inverse pole figure orientation maps taken from two different regions of the sample. The mapped regions contained a combination of the parent and transformed δ grains. The δ grain orientations are shown on discrete pole figures in Fig. 8(b). Several of the transformed δ grains exhibited similar orientations as indicated by the color-coded map and discrete pole figures. For example, the orientations of the red and gray marked grains of Fig. 8(a), which were on opposite ends of the same parent δ grain (blue), were within 10° of each other as analyzed by EBSD. The orientations of the neighboring brown and green marked grains were within five degrees of each other and were separated by a low angle grain boundary. These observations

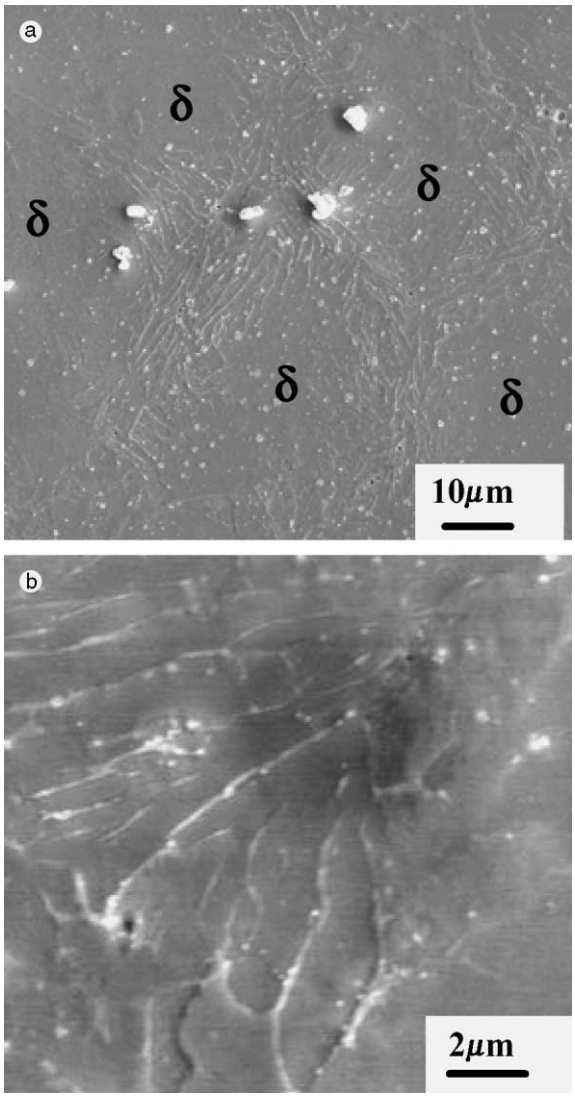

Fig. 5. SEM images of the ion-sputtered microstructure. The parent δ-phase grains are labeled in the (a) low-magnification image and a transformed region is exhibited in the (b) higher-magnification image.

imply that the transformed grains may have formed from the same ε grain orientation (i.e. they formed from the same ε grain or different ε grains of the same orientation).

EBSPs were successfully captured after the sample remained in the SEM chamber for more than 96 h, indicating that the vacuum environment was sufficient to prevent the buildup of a thick oxide layer. Combining this observation with those for the air transfers, the effect of environment on surface oxidation is emphasized, and this indicates the importance of maintaining a high-vacuum atmosphere after surface cleaning.

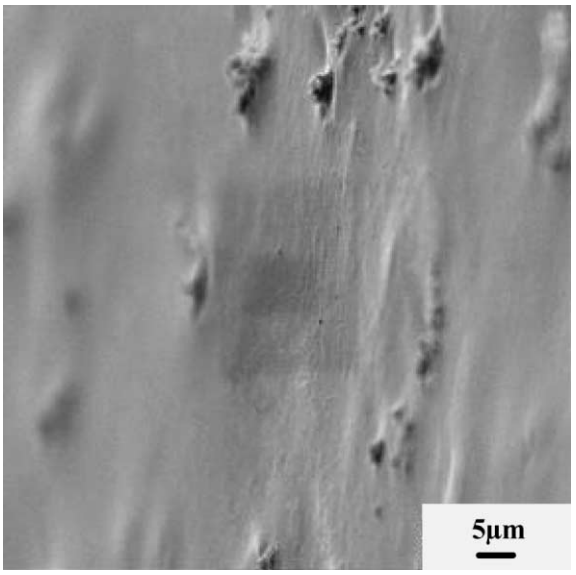

Fig. 6. SEM image of a region in which EBSD orientation maps were obtained. Note that shadowed rectangular area was a result of the electron beam scanning over the rectangular area mapped using a step size of 1 μm. The region of uneven surface topography, which was caused by electropolishing and ion-etching, surrounding the central area was avoided. Note that the sample normal was tilted 70° with respect to the electron beam.

4. Discussion

4.1. Technique

Samples exposed to the atmosphere just prior to SEM entry did not produce EBSPs of the Pu–Ga metal. This was attributed to the thick amorphous surface oxide layer that forms as a result of air exposure [1,3] as depicted in Fig. 2. Samples transferred through air included both as-electropolished samples that were not ion-sputtered as well as-electropolished then ion-sputtered samples. Note that the vacuum suitcase was not used to transfer such samples. Even an atmospheric exposure of only one second after ion-sputtering led to a surface that did not exhibit EBSPs of the underlying metal. EBSPs of the δ grains were obtained only after sputtering and sample vacuum transfer from the SAM to the SEM. Based on the relationship between characteristic depth from which backscatter electrons (BSEs) can be emitted and accelerating voltage [16], and taking into account the angle in which the incident electrons enter the sample surface, the characteristic depth from which BSEs can be emitted before being inelastically scattered is approximately 3 nm at 30 keV accelerating voltage for δ-Pu ($\rho = 15.92$ g/cm^3). Using inelastic mean-free path theory, it is expected that 95% of the incident electrons would experience an inelastic collision within 9 nm of the surface. Thus the bulk of the EBSD information on Pu is expected to come from the top several nanometers of the surface, thereby requiring that the surface oxide layer be quite shallow.

Accelerating voltage and beam current play important roles in terms of the quality and spatial resolution of EBSPs. A high beam current in small spots at low accelerating voltages is the domain of the FE SEM. However, drawbacks of low accelerating voltages are the susceptibility to stray magnetic fields and the high liability of pattern quality to preparation artifacts or foreign surface layers. Thus for Pu, low accelerating voltages are not attractive due to the difficulty in avoiding surface oxide layers. Higher accelerating voltages are beneficial due to their ability to allow a greater number of elastically scattered BSEs from greater depths. Thereby through higher accelerating voltage, the BSEs providing EBSD information have a greater likelihood to be from the underlying crystalline metal. It is therefore obvious that a sampling depth greater than the thickness of an impurity or a sputter-disordered layer is required. This emphasizes the surface sensitive nature of EBSD and thereby requires that the surface oxide and/or sputter-disordered layer for Pu be quite shallow. On the other hand, the quality of EBSPs depends upon the beam current. Larger beam currents give stronger signals but also correspond to larger probe sizes and therefore reduce spatial resolution [17]. Thus, there is a trade off between EBSP quality and spatial resolution. The limitations of the cold FE SEM used for this study included a maximum accelerating voltage of 30 keV and 12 μA emission current. The latter resulted in only 1–3 nA of specimen absorbed current, which is orders of magnitude smaller than that achievable with tungsten (W) or lanthanum hexaboride (LaB_6) sources and also hot Schottky FE SEMs.

Ion-etching is a useful practice for cleaning samples prior to EBSD analysis [11,17]. However, most materials are typically transferred from the ion-etcher through air to the SEM chamber. For extremely reactive metals, such as Pu and Ce, this jeopardizes the surface integrity. The sample vacuum transfer device was used to overcome this obstacle. To bypass the sample transfer step, however, the sample may be sputtered inside the SEM chamber. This has been successfully performed on the zircon ($ZrSiO_4$) system where EBSPs were achieved immediately after ion-cleaning the surface in a SEM chamber [18]. In the current case this would lead to severe radioactive contamination within the SEM chamber. However, an ultra-high vacuum SEM system containing an ion-gun and dedicated for radioactive materials analysis may be an effective instrument for obtaining high quality EBSPs of Pu alloys.

Impurity locations tended to sputter at a slower rate than the δ-phase metal, resulting in surface protrusions

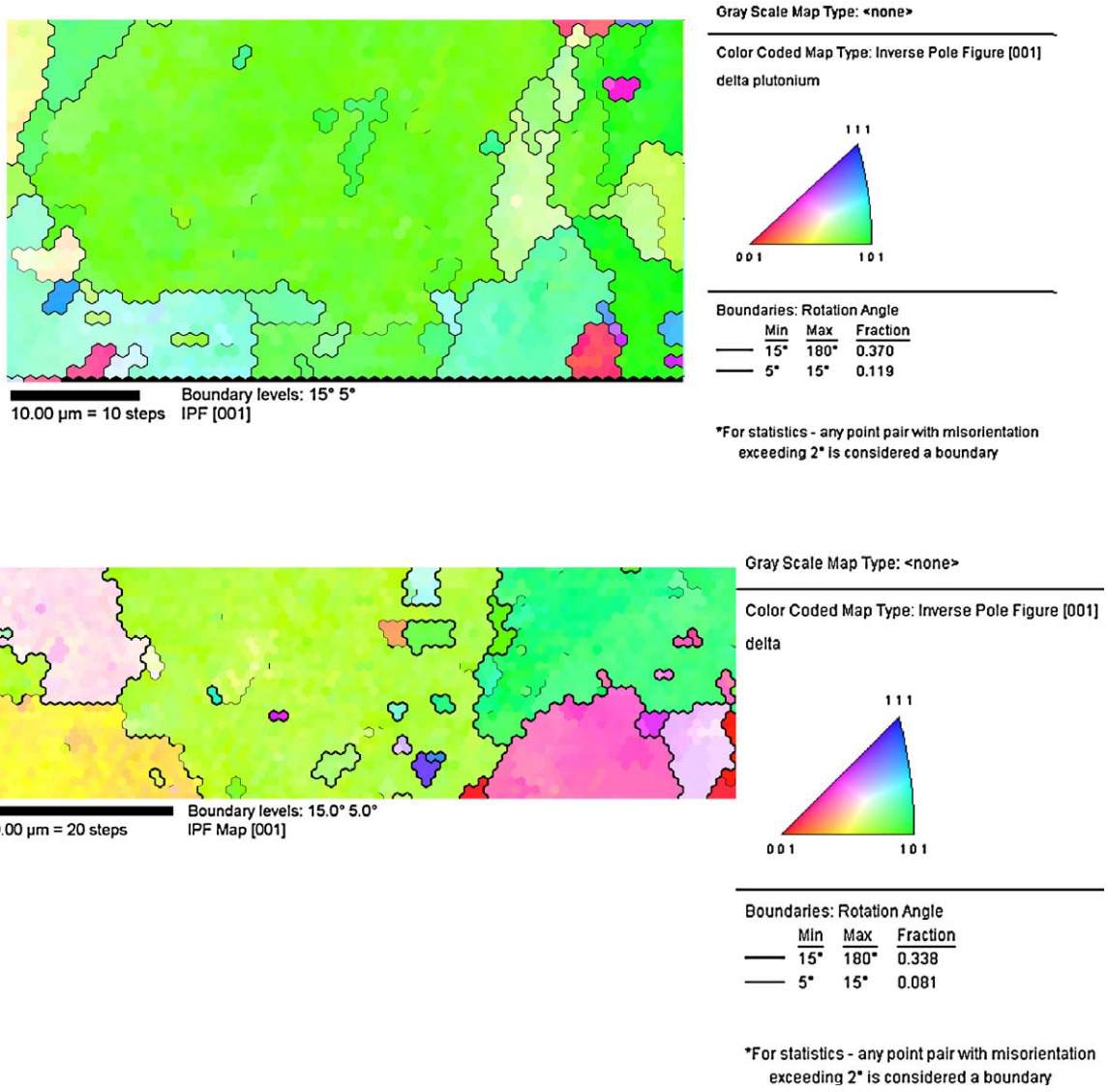

Fig. 7. Normal-direction inverse pole figure maps for two different regions of the sample where the colors represent the sample's normal direction indexed to the fcc unit triangle.

(see Fig. 6). The longer the sample is exposed to air the greater the surface oxide build up (for example see Ref. [14]), and therefore a longer sputtering time is necessary to clean the surface. This in turn causes greater surface topography degrading the accuracy and quality of the EBSP capture. For the current sample, which was transferred from the electropolisher to the SAM within minutes, the total sputtering time used to clean the surface was 20 min and less than 0.5 μm of the top surface was removed. A sputtering time of two hours was used for a previous sample [13], which was not transferred immediately after electropolishing to the SAM. Fig. 9(a) and (b) compare the microstructures of the samples sputtered for different durations. EBSPs were captured and indexed within the relatively flat regions of both microstructures depicted in Fig. 9, but they were not obtained when the beam was placed directly on the large protrusions of the 2-h sputtered sample. The protrusions also caused shadowing of the electron beam, making analysis of nearby regions difficult. Protrusions extending up to 30 μm have been observed after more than 10 h of ion-sputtering a Ce sample which had been exposed to air for several hours prior to ion-sputtering [14]. Thus by minimizing the

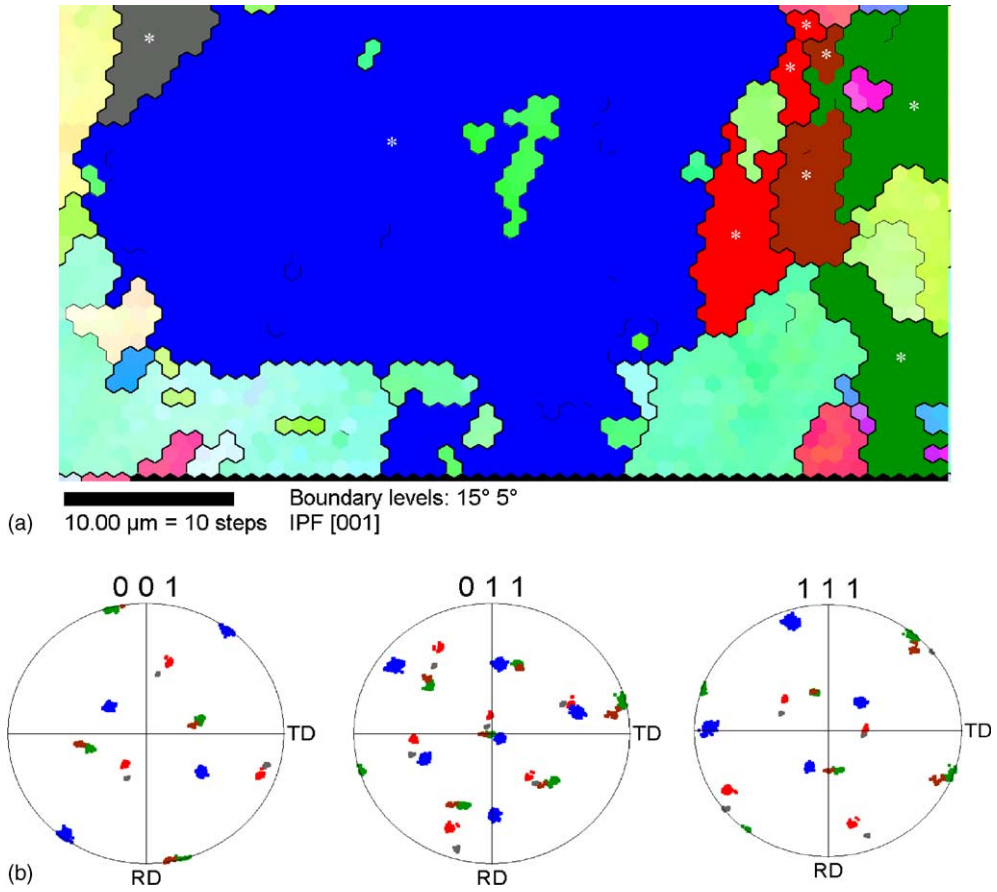

Fig. 8. An (a) orientation map where the orientation component of the marked grains (∗) is highlighted by color according to the discrete pole figures illustrated in (b). The grain misorientation tolerance was 5°.

total sputtering time, a significant reduction in the height of the protrusions is observed and this greatly increases the ability to obtain quality EBSD orientation maps. Overall, minimization of air exposure will benefit EBSD mapping, and it is suggested that oxidizing environments should be avoided during all sample preparation operations for Pu–Ga alloys.

4.2. Microstructural observations

The phase evolution of this alloy included a transformation to ε from the parent δ-phase followed by a transformation to the δ phase from the ε phase. A δ–ε orientation relationship cannot be confirmed by the EBSD analysis due to lack of orientation information from the body-centered-cubic (bcc) ε structure, which cannot be stabilized at RT for Pu–Ga alloys nor has it been successfully quenched to RT [19]. However, the proximity of each of the marked grains in Fig. 8 to the $\langle 0\,1\,1\rangle$ type orientation suggests that the variants formed from these grains could satisfy the Nishiyama–Wasserman relationship:

$$(1\,1\,0)_{\mathrm{bcc}} \| (1\,1\,1)_{\mathrm{fcc}}, \quad [0\,0\,1]_{\mathrm{bcc}} \| [-1\,0\,1]_{\mathrm{fcc}}$$

or the Kurdjumov–Sachs relationship:

$$(1\,1\,0)_{\mathrm{bcc}} \| (1\,1\,1)_{\mathrm{fcc}}, \quad [0\,0\,1]_{\mathrm{bcc}} \| [0\,-1\,1]_{\mathrm{fcc}}$$

These relationships are found between the fcc and bcc crystal systems of iron and other metals, and the only difference between the two is a rotation in the closest-packed planes of 5.26° [20–23]. Thus, this classic fcc/bcc orientation relationship could explain the observed variants of the transformed grains which resulted from the δ-to-ε-to-δ transformation. This orientation relationship has not been verified for the Pu–Ga system, one reason being the difficulty in obtaining the two-phase δ + ε microstructure at RT due to the large thermodynamic instability of the ε phase upon cooling.

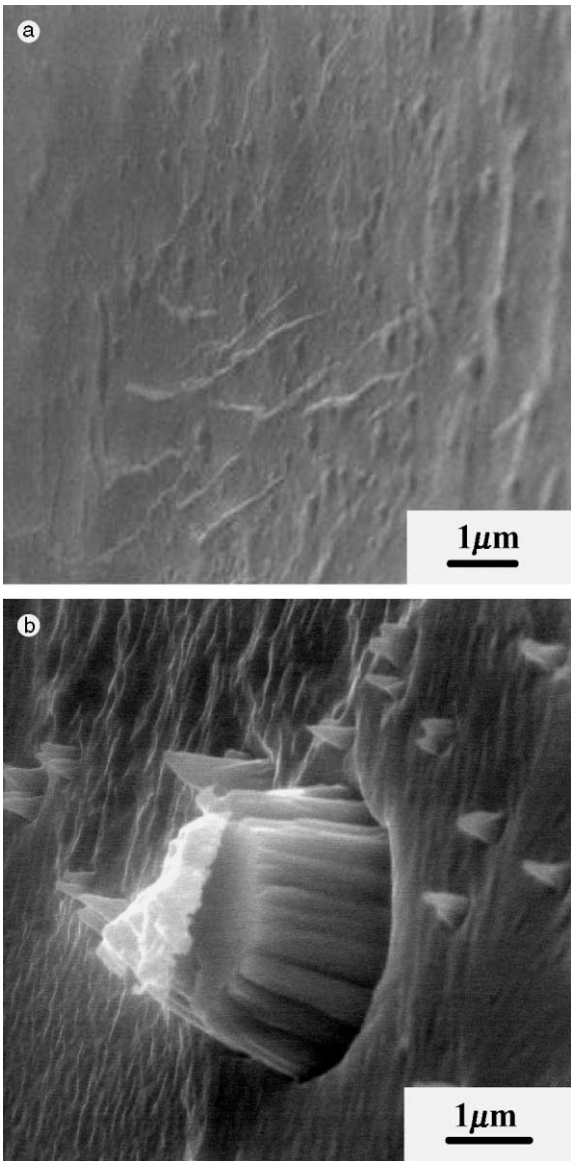

Fig. 9. SEM images of microstructures which have been ion-sputtered for a total time of (a) 20 min and (b) 2 h. Minimizing the total sputtering time required to clean the sample surface, which is related to the duration in which the sample was exposed to the atmosphere, results in less surface topography which is beneficial for obtaining quality EBSD orientation maps. Note that the sample normal was tilted 70° with respect to the electron beam.

5. Summary

This work represents the first successful attempt to obtain qualitative orientation maps for a Pu–Ga alloy using EBSD. EBSP capture of the Pu–Ga metal, which is extremely sensitive to surface oxidation, was unsuccessful for samples exposed to an atmospheric air environment. Sputter cleaning of the sample surface with Ar ions using a scanning Auger microprobe was necessary to remove the surface oxide and other surface contaminates, and transferring the cleaned sample to the SEM in a vacuum suitcase was necessary to maintain the integrity of the surface for successful EBSP capture. The EBSD observations provided some evidence for the δ–ε phase transformation behavior. This demonstrated sample preparation and characterization technique is expected to be a powerful means to further understand phase transformation behavior, orientation relationships, and texture in the complicated Pu and Pu-alloy systems.

Acknowledgements

Work was performed under the auspices of the US Department of Energy by Los Alamos National Laboratory under contract number W-7405-ENG-36. The authors are grateful to Mr Jeff Archuleta for aiding in the design and construction of the specimen vacuum transfer device and Mr John Bingert for assistance with data analysis.

References

[1] R.G. Haire, J.M. Haschke, MRS Bull. 26 (9) (2001) 689.
[2] I.A. Tsarenko, V.F. Serik, V.V. Titov, V.S. Akishin, V.A. Khokhlov, Atom. Energy 89 (6) (2000) 954.
[3] J.M. Haschke, T.H. Allen, J.L. Stakebake, J. Alloy. Compd. 243 (1996) 23.
[4] J.N. Mitchell, F.E. Gibbs, T.G. Zocco, R.A. Pereyra, Metall. Trans. 32A (2001) 649.
[5] T.G. Zocco, R.I. Sheldon, J. Nucl. Mater. 183 (1991) 80.
[6] T.G. Zocco, M.F. Stevens, P.H. Adler, R.I. Sheldon, G.B. Olson, Acta Metall. Mater. 38 (11) (1990) 2275.
[7] T.G. Zocco, R.I. Sheldon, M.F. Stevens, H.F. Rizzo, J. Nucl. Mater. 165 (1989) 238.
[8] T.G. Zocco, D.L. Rohr, Mater. Res. Soc. Symp. Proc. 115 (1988) 259.
[9] R.L. Moment, in: W.M. Miner (Ed.), Proceedings of Fourth International Conference on Plutonium and Other Actinides, Part I, The Metallurgical Society of the American Institute of Mining, Metallurgical, and Petroleum Engineers, New York, 1970, p. 457.
[10] B.L. Adams, S.I. Wright, K. Kunze, Metall. Trans. 24A (1993) 819.
[11] A.J. Schwartz, M. Kumar, B.L. Adams (Eds.), Electron Backscatter Diffraction in Materials Science, Kluwer Academic/Plenum, New York, 2000.
[12] D.E. Peterson, M.E. Kassner, Bull. Alloy Phase Diag. 9 (1988) 261.
[13] C.J. Boehlert, R.K. Schulze, J.N. Mitchell, T.G. Zocco, R.A. Pereyra, Scrip. Mater. 45 (9) (2001) 1107.

[14] C.J. Boehlert, J.D. Farr, R.K. Schulze, R.A. Pereyra, J.A. Archuleta, W.L. Hults, Philos. Mag. A, in press.
[15] J.F. Ziegler, J.P. Biersack, U. Littmark, The Stopping and Range of Ions in Solids, Pergamon, Oxford, 1985.
[16] D. Briggs, M.P. Seah, Practical Surface Analysis, second Ed., Auger and X-ray Photoelectron Spectroscopy, vol. 1, John Wiley, New York, 1990, p. 207.
[17] J.I. Goldstein, D.E. Newbury, P. Echlin, D.C. Joy, A.D. Romig Jr., C.E. Lyman, C. Fiori, E. Lifshin, Scanning Electron Microscopy and X-ray Microanalysis, 2nd Ed., Plenum, New York, 1992, p. 820.
[18] D.J. Dingley, K.Z. Baba-Kishi, V. Randle, Atlas of Backscattering Kikuchi Diffraction Patterns, Institute of Physics, Philadelphia, PA, 1995, p. 119.
[19] F.H. Ellinger, C.C. Land, V.O. Struebing, J. Nucl. Mater. 12 (2) (1964) 226.
[20] D.A. Porter, K.E. Easterling, Phase Transformations in Metals and Alloys, Van Nostrand Reinhold, Berkshire, England, 1981, p. 148.
[21] G. Kurdjumv, G. Sachs, Z. Phys. 64 (1930) 325.
[22] Z. Nishiyama, Sci. Rep. Tohoku Univ. 23 (1934) 637.
[23] G. Wasserman, K. Mitt. Wilh. Inst. Eisenforch. 17 (1935) 49.